Journal of Solid State Chemistry 305 (2022) 122670

Contents lists available at ScienceDirect

Journal of Solid State Chemistry

journal homepage: www.elsevier.com/locate/jssc

A diagnosis approach for semiconductor properties evaluation from ab initio calculations: Ag-based materials investigation

Luis Henrique da Silveira Lacerda [a,*], Elson Longo [b], Juan Andrés [c], Miguel Angel San-Miguel [a]

[a] State University of Campinas, Campinas, São Paulo, Brazil
[b] CDMF-UFSCAR, Federal University of São Carlos, São Carlos, São Paulo, Brazil
[c] University Jaume I, Castellón, Spain

ARTICLE INFO

Keywords:
Electronic structure
Photocatalysis
Semiconductors
DFT
Biocide

ABSTRACT

Ag-based semiconductors have been extensively employed as photocatalysts for several decades due to their excellent electronic properties, photochemical properties, and relatively low synthesis cost. In this work, the α-Ag_2WO_4, β-Ag_2WO_4, γ-Ag_2WO_4, α-$AgVO_3$, β-$AgVO_3$, α-Ag_2MoO_4, β-Ag_2MoO_4, Ag_2CrO_4, and Ag_3PO_4 materials were systematically investigated by DFT/B3LYP calculations. The structural features were described by cations coordination, cluster distortion degree, and structure formers and modifiers. In turn, the evaluation of electronic properties indicates band gap values in the range of 2.54 eV–4.32 eV. The calculated density of charge carriers shows that the holes are the predominant charge carrier for all evaluated semiconductors, except for α-Ag_2MoO_4. The effective masses of charge carriers were also computed, and good stability for generated electrons and holes are expected for α- and β-Ag_2WO_4, α-$AgVO_3$, β-$AgVO_3$, β-Ag_2MoO_4, Ag_2CrO_4, and Ag_3PO_4 materials. Finally, the valence and conduction band edge potentials point to the Ag-based semiconductors as promising candidates for photocatalytic and biocide activities.

1. Introduction

The modern human society enjoys different privileges arising from fast technological advance which is strongly associated to novel functional materials [1–4]. The solid-state materials responsible for such technological developments are related to the presence of relevant electronic, optical, ferroelectric, magnetic, and other properties. In this context, semiconductor materials stand out as materials that offer such properties being successfully used for technological applications and produced on a large scale and low economic cost [5,6]. In particular, the interest in semiconductors has increased drastically due to i) their potential to treat water effluents contaminated with organic pollutants through a photocatalytic process [7–9] and ii) biocide activity aiming to minimize the dissemination of the disease [10,11].

Over the last years, novel semiconductor materials with excellent properties have been proposed. Among such materials stands out the Ag-based semiconductors which present unique electronic, photocatalytic, and biologic properties. For this reason, our research group has devoted much effort to studying this class of materials characterizing different properties and unveiling their physical-chemical principles from theoretical approaches. The main Ag-based semiconductors are discussed below. The Ag_2WO_4 is a semiconductor observed in three different polymorphs, being the α structure (Pnn2) the most stable while the β (P63/m) and γ (Fd-3m) are meta-stable phases [11]. Silva et al. [12] reported ozone gas-sensors based on one-dimensional α-Ag_2WO_4 nanostructures. Similarly, Laier et al. [13] have studied the surface dependency of the properties for the same polymorph. Other works focused on Ag_2WO_4 have investigated their antitumor and antifungal activities [14,15], photoluminescence [16–20], different synthesis techniques [21,22], antibacterial potential [23–25] and photocatalytic properties [23,26]. The Ag_3PO_4 has also been extensively investigated, and their photocatalytic [27–30], electronic [31–35], antiviral and antibacterial [36] properties reported.

The $AgVO_3$ also presents polymorphic behavior and has attracted attention due to its higher biocompatibility and minor Ag amount in the formula unit [37]. Other studies on $AgVO_3$ properties depict their structural stability [38], photoluminescence [39,40], and antibacterial features [41]. In turn, the Ag_2MoO_4 polymorphs were described by means of electronic structure [42], photoluminescence [43], optical properties [44], and antibacterial activity [45,46]. Meanwhile, the Ag_2CrO_4 is a recently investigated semiconductor aiming its application as a photocatalyst [47–49] and biological agent [50].

* Corresponding author.
E-mail address: lhslacerda1@gmail.com (L.H.S. Lacerda).

https://doi.org/10.1016/j.jssc.2021.122670
Received 10 August 2021; Received in revised form 14 October 2021; Accepted 15 October 2021
Available online 18 October 2021

In this work, the α-Ag_2WO_4, β-Ag_2WO_4, γ-Ag_2WO_4, α-$AgVO_3$, β-$AgVO_3$, α-Ag_2MoO_4, β-Ag_2MoO_4, Ag_2CrO_4, and Ag_3PO_4 materials were carefully investigated through ab initio simulations depicting their crystalline features and electronic structures. As well, some relevant insights into possible photocatalytic and biocide potential are presented.

2. Computational details

In this work, the photocatalytic potential of Ag-based semiconductors was evaluated by DFT simulations [51,52] The α-Ag_2WO_4, β-Ag_2WO_4, γ-Ag_2WO_4, α-$AgVO_3$, β-$AgVO_3$, Ag_2MoO_4, Ag_2MoO_4, and Ag_2CrO_4 were simulated using periodic models constructed from experimental crystalline data [11,39,42,44,49,53]; these materials possess Pn2n, P63/m, Fd3m, Cd/c, Cm, Pbca, P4122, Fd-3m, and Pnma space groups, respectively. Fig. 1 presents the unit cell for all investigated Ag-based materials.

The constructed models were fully optimized and discussed in terms of structural, electronic, and photocatalytic properties. The geometry was evaluated regarding the lattice parameters, bond-lengths, and [AgO_x] and [MO_x] clusters as building blocks of the α-Ag_2WO_4, β-Ag_2WO_4, γ-Ag_2WO_4, α-$AgVO_3$, β-$AgVO_3$, α-Ag_2MoO_4, β-Ag_2MoO_4, Ag_2CrO_4, and Ag_3PO_4 materials. The electronic structure was analyzed from the total density of states (DOS) projections, band structure (BS) profiles, and the semiconductor type. The last one was estimated from the Fermi distribution on the top of the valence band (VB) and the bottom of the conduction band (CB). The DOS and BS analysis was performed for the last five bands of VB and the first five bands of CB, covering the band gap region. In turn, the photocatalytic properties were determined by the mobility of the charge carriers and the ability to oxidize or reduce H_2O and O_2 molecules.

The simulations employ the density functional theory (DFT) allied to the B3LYP hybrid functional using the CRYSTAL17 [54] package. The B3LYP functional employed in this work is the default version available on CRYSTAL code, including the Slater exchange correction combined with the fifth version of Vosko, Wilk, Nusair correlation description (SVWN5). This exchange-correlation functional offers an excellent prediction of materials properties allied to a relatively low computational cost compared to other hybrid functionals such as HSE06 and WC1LYP [55–57]. Furthermore, the Grimme dispersion-corrections [58,59] were also taken into account for all models since our previous report [60] evidences that such corrections are essential to better describe the Ag-based structural features. The calculations employ SCF convergence criteria established as 10^{-8} and Mohnkhorst-Pack method [61,62] for k points grid defined as 8 × 8 × 8. The parameters above guarantee high reliability in the results, mainly for electronic structure prediction. The Ag, W, V, Mo, Cr, and O atoms were described by Gaussian-type basis sets reported in references [63–68].

3. Results and discussion

3.1. Structural evaluation

The structural properties of the investigated Ag-based semiconductors were discussed in terms of lattice parameters, unit cell volume, and cluster description. The calculated values for the unit cell (Table 1) agree with experimental measurements [69–71], indicating the reliability of our methodology. As observed, the calculated lattice parameters and unit cell volumes are very similar to XRD results for all materials. Table 2 presents detailed information about the clusters within the structure, displaying the cation coordination numbers, Ag – O and M – O (M = W, V, Mo, Cr, and P) bond lengths, and the distortion degree (Δ) for each cluster (Table 2). The Δ value for a cluster as expressed in Equation (1) relates the bond length (d_i), the average bond distance (d_{ave}), and the cation coordination number (c_n).

$$\Delta = \frac{1}{c_n}\sum_i \left\{ \frac{(d_i - d_{ave})^2}{d_{ave}} \right\} \quad (1)$$

First of all, the Ag_2WO_4 polymorphs were discussed; the α polymorph presents four different [AgO] clusters, where the c_n for Ag is 2, 4, 6, and 7 and three different distorted [WO_6] octahedra. The β polymorph for Ag_2WO_4 exhibits [AgO_6], [AgO_5], [WO_5], and [WO_4] clusters, being the penta-coordinated sites more distorted, mainly for [WO_5]. In contrast, non-distorted [AgO_6] and [WO_6] clusters are observed in the gamma phase. It is essential to highlight that the β and γ phases are metastable [11,20]. As observed for γ-Ag_2WO_4, the Ag_3PO_4 presents perfect tetrahedral sites composed of Ag and P.

In the case of $AgVO_3$ materials, the α polymorph presents two distinct [AgO_6] clusters and one type of [VO_4] cluster; both clusters show a high distortion degree. The β polymorph possesses two different distorted [VO_6] sites and also distorted [AgO_6], [AgO_5], [AgO_6] clusters. In contrast to Ag_2WO_4, both polymorphs of $AgVO_3$ are stable and synthesized from different approaches. The Ag_2MoO_4 materials were also investigated, and the obtained results indicate the existence of perfect [AgO_6] and [MoO_4] clusters in the β phase. Thus, the α polymorph exhibits highly distorted [AgO_4] tetrahedra, two different types of distorted [AgO_6] and distorted [MoO_6] clusters. Finally, the Ag_2CrO_4 possesses slightly distorted tetrahedral Cr sites and two distinct six-folded Ag sites with high distortion.

Another relevant discussion is the role of the different [AgOx] and [MOx] clusters in forming the crystal structure and classified as structure formers or structure modifiers [72]. The structure formers are the clusters responsible for creating the crystalline network; these clusters are usually composed of chemical bonds with more pronounced covalent behavior [73]. In turn, the structure modifiers refer to those clusters responsible for connecting different crystalline structures, enabling polymorphism, and are commonly composed of chemical bonds with major ionic character [74]. In the case of Ag-based semiconductors, Botelho et al. [75], Longo et al. [17], and Gouveia et al. [43] stated that the [AgO_x] clusters act as structure modifiers in Ag_3PO_4 and Ag_2MoO_4 materials. Similarly, the structural results presented in this work point out that such clusters also play the role of modifier for Ag_2WO_4, $AgVO_3$, and Ag_2CrO_4 due to the high distortion degree in the [AgO_x] polyhedra. Further, the different Ag coordination observed in different polymorphs corroborates the role of [AgO_x] as a structure modifier, whereas the [MO_x] clusters behave as structure formers in the investigated Ag-based materials.

Furthermore, from the evaluation of structural features, it is possible to access essential insights into materials properties since Ag and M species existence in different chemical environments leads to different electronic structures and stability. The comparison between distortion degrees (Table 2) and band gap values (Table 4) indicates that the polymorphs with high distortion degrees present narrowed band gap values. A similar observation was reported for $CdGa_2S_4$, $CdGa_2Se_4$, $CdGa_2Te_4$, and Na-doped $CuInS_2$ materials [76,77]. The distortion degree for [AgO_x] and [MO_x] clusters is also connected to the polymorphs energies, being higher total energies (E_T) found for high-distorted systems. The stability predicted from E_T disagreed with the experimental reports for the polymorphs; however, the proper prediction of polymorph stability requires phonon calculations and phase transitions investigations which are far from the focus of this work.

The theoretical results presented in this work also offer important insights into the crystalline structure of Ag-based semiconductors previously synthesized by our group. The previous manuscripts [11–24,26,32,37–47,50,60,75,78–89] focused on describing the lattice parameters allied to cluster coordination. Thus, this work provides a complete description of the crystalline structures, discussing cluster coordination and its quantitative distortion degree, lattice parameters, bond lengths, and structure formers and modifiers.

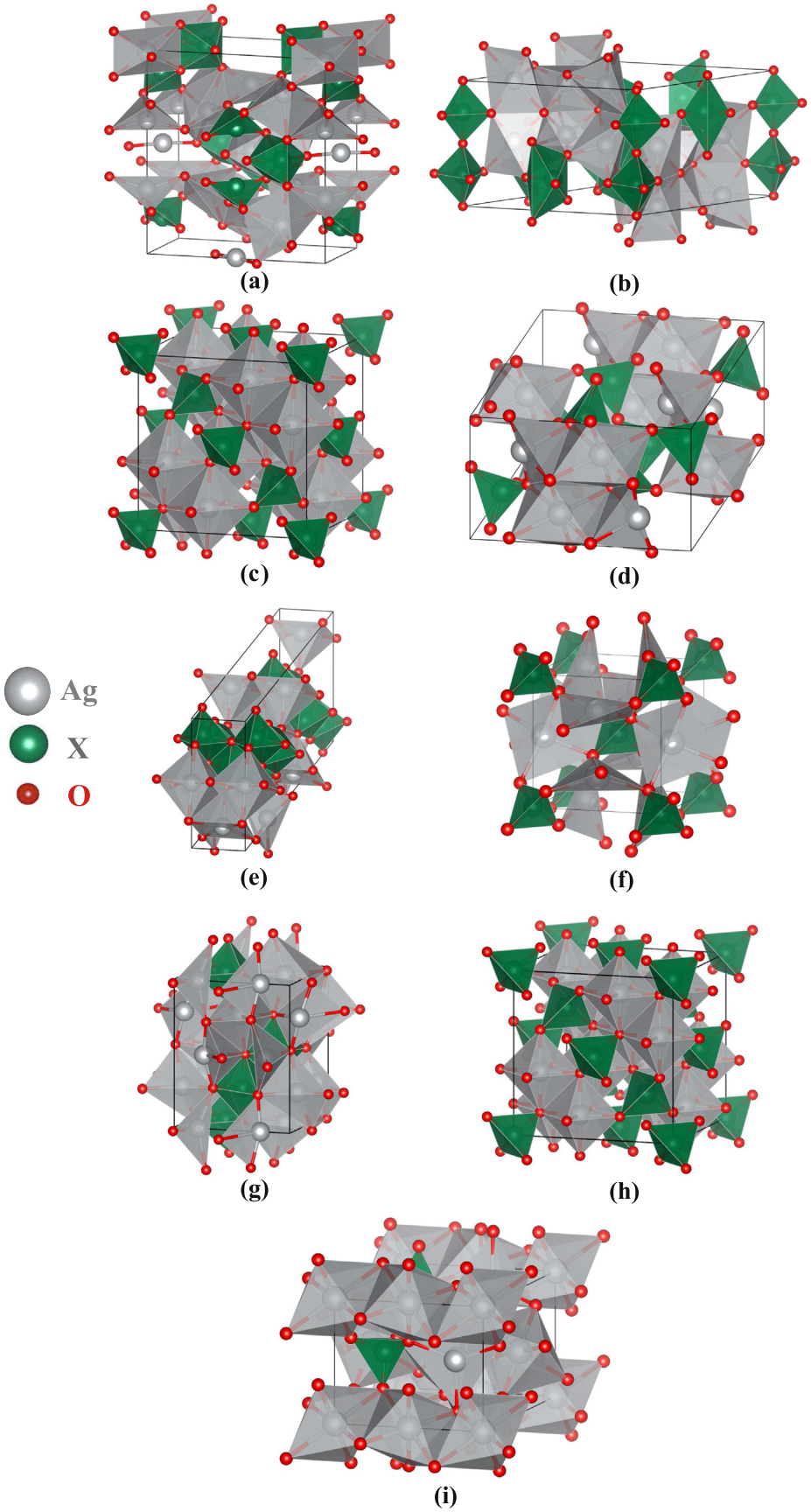

Fig. 1. Schematic representation of 3D structures of (a) α-Ag_2WO_4, (b) β-Ag_2WO_4, (c) γ-Ag_2WO_4, (d) α-$AgVO_3$, (e) β-$AgVO_3$, (f) Ag_3PO_4, (g) α-Ag_2MoO_4, (h) β-Ag_2MoO_4 and (i) Ag_2CrO_4. The [AgO_x] and [MO_x] clusters are depicted.

Table 1
Lattice parameters and unit cell volume for investigated Ag-based semiconductors.

		Space group	Lattice Parameters						
			a (Å)	b (Å)	c (Å)	α (°)	β (°)	γ (°)	V (Å^3)
α-Ag_2WO_4	This work	**Pn2n**	5.813	11.133	12.358	90	90	90	799.85
	Exp [70].		5.92	10.89	12.03	90	90	90	775.56
β-Ag_2WO_4	This work	**P63/m**	11.077	11.077	7.60	90	90	120	806.98
	Exp [70].		11.09	11.09	7.54	90	90	120	803.71
γ-Ag_2WO_4	This work	**Fd-3m**	9.496	9.496	9.496	90	90	90	846.47
	Exp [69].		9.33	9.33	9.33	90	90	90	812.16
α-$AgVO_3$	This work	**C2/c**	10.580	9.685	5.696	90	101.21	90	568.46
	Exp [70].		10.44	9.90	5.53	90	99.7	90	563.30
β-$AgVO_3$	This work	**Cm**	17.942	3.537	8.270	90	103.70	90	509.88
	Exp [70].		18.11	3.58	8.04	90	104.40	90	504.70
α-Ag_2MoO_4	This work	**P4122**	7.115	7.115	7.115	90	90	90	455.54
	Exp [71].		7.01	7.01	7.01	90	90	90	424.93
β-Ag_2MoO_4	This work	**Fd-3m**	9.533	9.533	9.533	90	90	90	866.28
	Exp [70].		9.32	9.32	9.32	90	90	90	808.80
Ag_2CrO_4	This work	**Pnma**	10.152	6.968	5.555	90	90	90	393.00
	Exp [70].		10.07	7.02	5.54	90	90	90	391.79
Ag_3PO_4	This work	**P-43n**	6.064	6.064	6.064	90	90	90	222.99
	Exp [70].		6.00	6.00	6.00	90	90	90	216.43

Table 2
Coordination number, bond lengths, total energy (E_T), and distortion degree (Δ) for [AgO_x] and [MO_x] clusters (M = W, V, Mo, Cr, and P) for the Ag-based semiconductors. The number in parentheses indicates the number of repetitions of a bond length.

	Cluster	Bond lengths (Å)	Δ (10^{-4})	E_T (Hartree)
α-Ag_2WO_4	[AgO_7]	2.33, 2.43, 2.50, 2.64, 2.65, 2.89, 3.04	49.13	−4.8021. 10^3
	[AgO_6]	2.33, 2.43, 2.50, 2.64, 2.65, 2.89	46.16	
	[AgO_4]	2.29 (2), 2.34 (2)	0.98	
	[AgO_2]	2.13 (2)	0	
	[WO_6]	1.75 (2), 1.82, 1.92, 2.32, 2.33	158.72	
	[WO_6]	1.75 (2), 1.85 (2), 2.39 (2)	198.44	
	[WO_6]	1.74 (2), 1.84 (2), 2.38 (2)	198.46	
β-Ag_2WO_4	[AgO_6]	2.37 (3), 2.51 (3)	5.32	−4.8033. 10^3
	[AgO_5]	2.32, 2.43, 2.57, 2.59, 2.89	55.85	
	[WO_4]	1.76 (2), 1.77, 1.78	0.21	
	[WO_5]	1.80 (3), 1.90 (2)	408.99	
γ-Ag_2WO_4	[AgO_6]	2.55 (6)	0	−1.2006. 10^3
	[WO_6]	1.77 (4)	0	
α-$AgVO_3$	[AgO_6]	2.33 (2), 2.40 (2), 2.57 (2)	17.57	−5.2621. 10^3
	[AgO_6]	2.24 (2), 2.54 (2), 2.72 (2)	62.37	
	[VO_4]	1.65, 1.66, 1.80, 1.81	18.62	
β-$AgVO_3$	[AgO_6]	2.35 (2), 2.44 (4)	3.03	−5.2621. 10^3
	[AgO_5]	2.42 (2), 2.46 (2), 2.54	3.07	
	[AgO_4]	2.31 (2), 2.74 (2)	74.11	
	[VO_6]	1.66, 1.70, 1.88 (2), 2.24, 2.33	171.18	
	[VO_6]	1.66, 1.72, 1.85 (2), 2.12, 2.46	196.98	
α-Ag_2MoO_4	[AgO_4]	2.21 (2), 2.94 (2)	202.66	−3.2233. 10^3
	[AgO_6]	2.38 (2), 2.54 (2), 2.76 (2)	37.78	
	[AgO_6]	2.47 (2), 2.58 (2), 2.74 (2)	18.92	
	[MoO_6]	1.90 (2), 2.00 (2), 2.09 (2)	14.88	
β-Ag_2MoO_4	[AgO_6]	2.54 (6)	0	−1.3200. 10^3
	[MoO_4]	1.81 (4)	0	
Ag_2CrO_4	[AgO_6]	2.35 (2), 2.38 (2), 2.60 (2)	21.52	−6.5476. 10^3
	[AgO_6]	2.30 (2), 2.42 (2), 2.49 (2)	10.93	
	[CrO_4]	1.65, 1.65 (2), 1.67	0.24	
Ag_3PO_4	[AgO_4]	2.39 (4)	0	−2.1592. 10^3
	[PO_4]	1.56 (4)	0	

3.2. Electronic structure

The electronic properties of Ag-based semiconductors investigated in this manuscript were described from the total DOS projection, BS, and electron-hole charge carriers properties. The DOS data (Fig. 2) for all semiconductors indicate that, despite the polymorphism, the chemical elements contribute similarly to the VB and CB. The W atoms have a reasonable contribution to VB states and substantial participation in the formation of CB; the V atoms contribute to VB energy levels and, more significantly, to CB. The Mo species compose the VB by a small contribution and are responsible for forming the CB. The Cr atoms also contribute to both regions, but the participation on CB is more pronounced. Meanwhile, the P species possess little contribution to VB and CB. In particular, the O atoms show a regular contribution to all investigated Ag-based semiconductors since they are relevantly involved in forming VB and CB energy levels, being the highest participation to the VB states. Finally, the Ag atoms also present a regular contribution to both energy regions on all investigated systems; for such atoms, a high contribution to VB is observed allied to a minor contribution to CB.

The BS profiles (Fig. 3) are also discussed, featuring the band gap region. The results indicate that the VB energy levels are located in a low energy range, being observed close to each other in terms of energy whereas the energy levels for CB are well-spaced from each other. The energy separation is more accentuated in β-Ag_2WO_4, α-Ag_2MoO_4, and Ag_3PO_4, where the investigated CB levels cover a more comprehensive energy range.

DOS analysis for Ag-based semiconductors allows estimating the charge carrier concentration through the Fermi distribution, which considers the temperature influence on the number of electrons and holes [5,90]. Mathematically, the Fermi distribution is represented by Equations (2) and (3), which relate the Boltzmann constant (k_b), temperature (T), electronic DOS per unit cell volume (D(ε)), Fermi energy level (ε_F), maximum VB energy value (ε_{VBM}) and minimum CB energy value (ε_{CBM}). This methodology assumes that the presence of dilute defects does not essentially affect the DOS and, consequently, the charge carrier density. From the obtained values, the semiconductor type can be determined. Thus, n-type semiconductors (electrons as predominant charge carrier) are associated with a higher number of states in CB. Likewise, an increased number of states in VB regions indicates a high possibility of photogenerated electrons, indicating a p-type semiconductor. The reliability of charge carriers density obtained from Fermi distribution is evidenced in references [91–95]. In this work, the charge carrier density was determined at 300 K, 600 K, and 900 K, and computed results compose Table 3.

$$p = \int_{-\infty}^{\varepsilon_{VBM}} D(\varepsilon) \frac{1}{exp^{[(\varepsilon_F - \varepsilon)/k_B T]} + 1} d\varepsilon \quad (2)$$

Table 3
Charge carrier concentration (expressed in 10^{22} cm^{-3}) for Ag-based semiconductors at 300 K, 600 K, and 900 K.

	Semiconductor type	300 K		600 K		900 K	
		holes	electrons	holes	electrons	holes	electrons
α-Ag_2WO_4	p	9.244	4.354	9.474	4.462	10.040	4.473
β-Ag_2WO_4	p	2.134	1.228	2.191	1.258	2.322	1.333
γ-Ag_2WO_4	p	1.302	1.131	1.334	1.159	1.414	1.228
α-$AgVO_3$	p	2.164	1.630	2.218	1.671	2.351	1.770
β-$AgVO_3$	p	2.177	1.867	2.232	1.914	2.365	2.028
α-Ag_2MoO_4	n	1.940	2.243	1.988	2.299	2.107	2.434
β-Ag_2MoO_4	p	1.311	1.228	1.344	1.258	1.424	1.333
Ag_2CrO_4	p	2.554	2.379	2.617	2.439	2.774	2.584
Ag_3PO_4	p	4.855	4.402	4.977	4.511	5.273	4.781

Table 4
Bandgap values and effective mass for charge carriers for investigated Ag-based semiconductors.

	Band-gap (eV)		Effective mass		
	This work	Exp.	m_{h^*}/m_o	m_{e^*}/m_o	m_{h^*}/m_{e^*}
α-Ag_2WO_4	3.02 (G – G)	3.10 [20]	0.65	0.41	0.64
β-Ag_2WO_4	3.16 (G – M)	3.10 [22]	30.88	10.07	0.33
γ-Ag_2WO_4	4.32 (G - SM)	3.21 [69]	29.57	35.26	1.19
α-$AgVO_3$	3.31 (B – G)	2.80 [41]	25.67	64.35	2.51
β-$AgVO_3$	3.00 (B – B)	2.04 [82]	48.00	23.06	0.48
α-Ag_2MoO_4	2.00 (G – Z)	1.26 [42]	7.90	9.24	1.17
β-Ag_2MoO_4	3.98 (G – G)	3.41 [46]	28.74	13.53	0.47
Ag_2CrO_4	2.69 (G – Z)	1.80 [47]	30.35	45.27	1.49
Ag_3PO_4	2.54 (M – G)	2.45 [87]	0.29	0.11	2.64

$$n = \int_{\varepsilon_{CBM}}^{\infty} D(\varepsilon) \frac{1}{exp^{[(\varepsilon - \varepsilon_F)/k_B T]} + 1} d\varepsilon \quad (3)$$

In summary, the results indicate an n-type semiconductor behavior for α- and β-Ag_2MoO_4 and a p-type semiconductor for the other evaluated materials. Moreover, the calculated values suggest a significant increase in charge carrier number as temperature increases, as expected for semiconductors. Although the materials discussed in this work have already been investigated in the literature, to the best of our knowledge, the semiconductor type was not determined by experimental or theoretical analysis. Therefore, our results represent the first evaluation of charge carrier concentration for α-Ag_2WO_4, β-Ag_2WO_4, γ-Ag_2WO_4, α-$AgVO_3$, β-$AgVO_3$, $Ag_4V_2O_7$, α-Ag_2MoO_4, β-Ag_2MoO_4, Ag_2CrO_4, and Ag_3PO_4 materials.

Further, the electronic structure has also been discussed regarding band gap values (Table 4), which suggest all materials as typically semiconductors with a band gap in the visible range of the electromagnetic spectrum (1.6 eV–3.3 eV), but β-Ag_2MoO_4 that has a band gap in the ultraviolet region. The band gap values agree with some previously reported experimental results, evidencing the theoretical methodology's reliability employed in this work [20,22,41,42,46,47,69,82,87]. The prediction of the band gaps from DFT simulation is always challenging since the obtained values might be far from the experimental values. For instance, LDA and PBE functionals usually provide metallic or conductor band gaps for semiconductor materials [55,60]. This failure can partially be avoided using the Hubbard parameter (U) that corrects the band gap description. Another alternative approach is the employment of hybrid exchange-correlations functionals [51,52]. Thus, the chosen DFT/B3LYP methodology in this work has been used successfully in other studies and adequately predicted the band gap of the semiconductor materials [1,96,97].

Furthermore, the reliability of the other analysis performed in this work is corroborated by our other works employing a similar theory level [60,95,98,99] or manuscripts from other authors [91–93,100,101]. In particular, the results of band edge potential for Ag-based semiconductors are also strong evidence of the reliability of the calculations since they agree with experimental reports.

Finally, from the band structure profiles, it is possible to determine the mobility of the charge carriers and the efficiency of the conduction process [5] using the effective mass method [102–105]. This method relates the mass of holes (m_{h^*}), electrons (m_{e^*}) and the invariant electron mass(m_o), being the mobility of the charge carrier predicted from the evaluation of the electron (m_{h^*}/m_o) and hole (m_{e^*}/m_o) effective masses. A qualitative evaluation of both charge carrier values can elucidate the efficiency of the materials in the conduction process if the dominant charge carrier presents low minor effective mass value [5]. Further, the ratio between charge carrier effective masses (m_{h^*}/m_{e^*}) enables to predict the recombination rate of the photogenerated electron-hole pairs; in general, a good photocatalytic activity is found in materials with m_{h^*}/m_{e^*} minor than 0.5 or higher than 1.5 [106–109]. The calculated results (Table 4) suggest an outstanding charge carrier mobility for Ag_3PO_4 allied to a moderate efficiency on the conduction process because of high mobility for electrons instead of holes. The same limited efficiency is observed for α-$AgVO_3$, which possesses moderated mobility of charge carriers. The other semiconductors investigated present moderated mobility associated with good efficiency in the conduction process since the predominant charge carrier is significantly more mobile than the other charge carrier.

3.3. Prediction of photocatalytic, antibacterial, and antiviral activities

Semiconductor photocatalysts are powerful alternatives to degrade water contaminants using solar radiation without generating other hazardous species, being used for such purposes for several decades. Usually, the photodegradation process catalyzed by semiconductors includes the following steps: i) sunlight absorption creates photogenerated electron-hole pairs; ii) charge carrier separation and electron transfer with chemical molecules absorbed on semiconductor surfaces; iii) charge carrier participation in oxidation/reduction process on the surface to generate reactive oxygen species (ROS), and iv) recombination of charge carriers in bulk or surface of the semiconductor [110]. Thus, the photocatalytic potential of semiconductor materials depends on the thermodynamics and kinetics of the process mentioned above and adequate band gap values (desired in the visible range) allied to good stability of charge carriers [106–109].

For the Ag-based semiconductors investigated in this work, the results (Table 3) suggest that $AgWO_4$, $AgVO_3$, Ag_3PO_4, and Ag_2CrO_4 possess an exciting combination of band gap and charge carriers stability; consequently, such semiconductors are potential candidates for photocatalytic-based purposes. Among such materials, the Ag_3PO_4 and Ag_2CrO_4 are highlighted since they possess band gaps similar to that value considered as the most efficient for photodegradation and water splitting processes (2.40 eV). Some works support this information showing that this band gap value is related to a minimum efficiency of 10% in the use of incident solar radiation [111,112]. As well as, previous results reported by our group evidences both materials as potential photocatalysts [87,113].

The insights on Ag-based semiconductors with photocatalytic potential can be expanded from the VB and CB edge potential analyses,

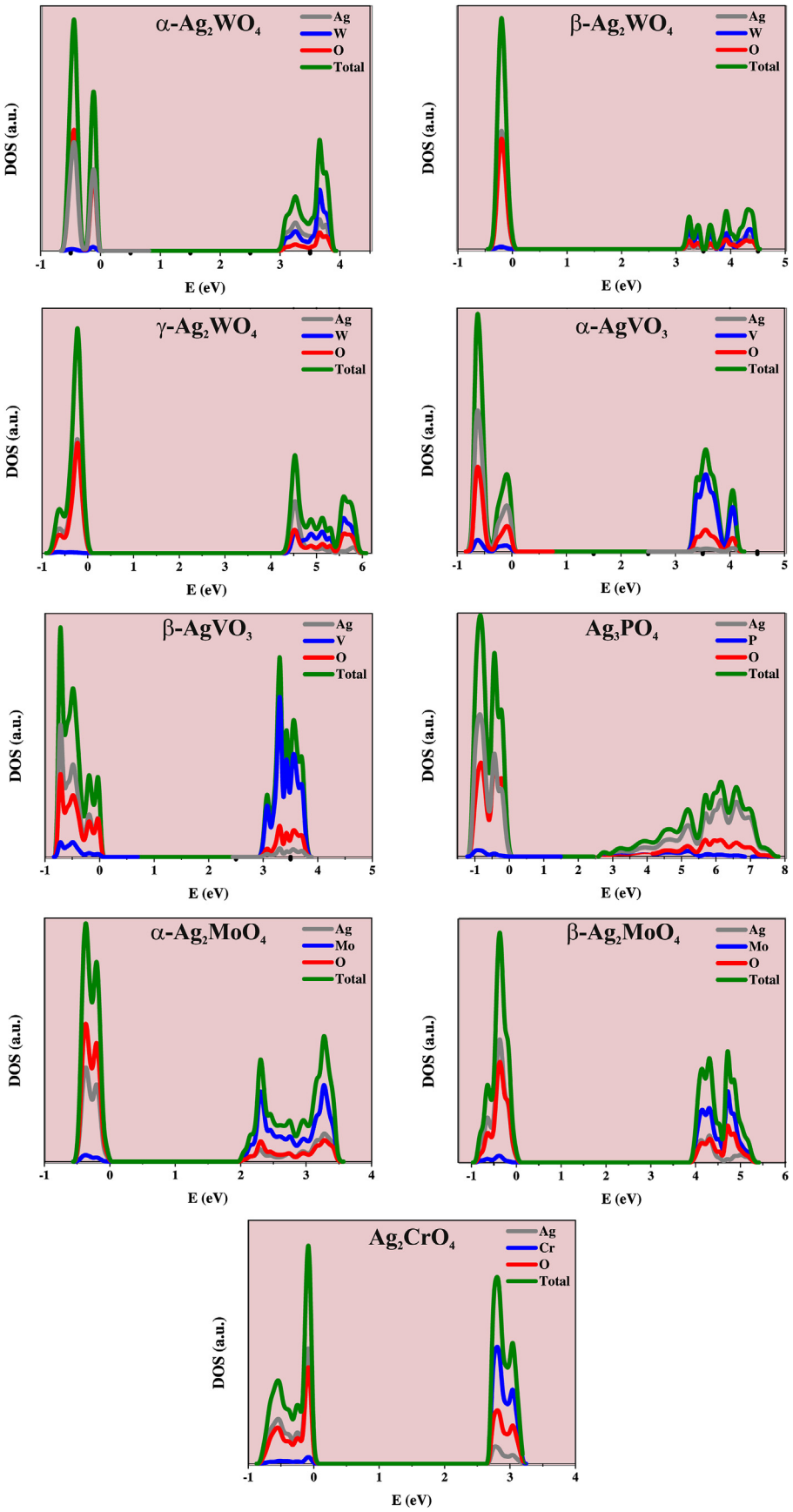

Fig. 2. The total density of states projection for Ag-based materials.

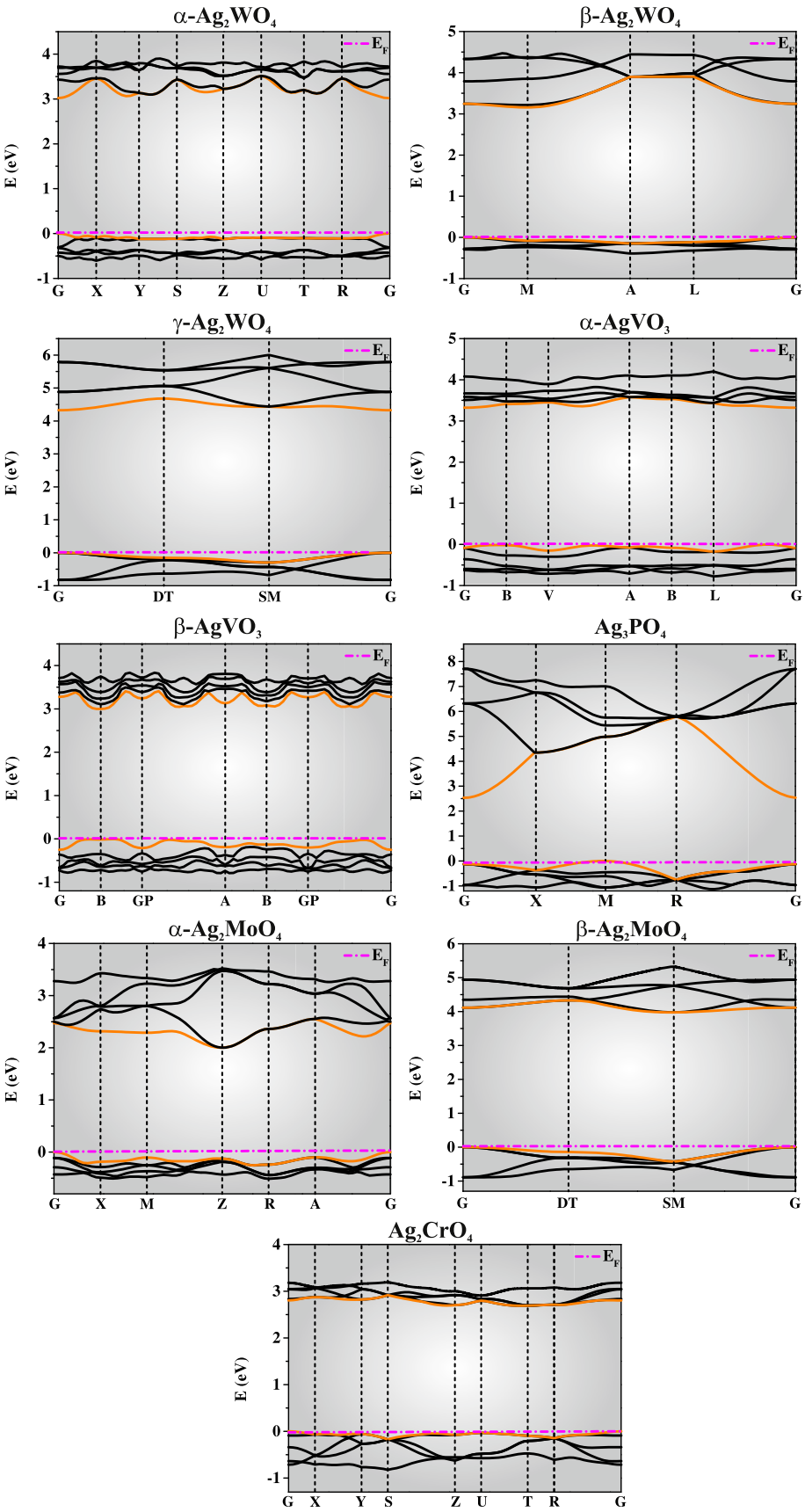

Fig. 3. Band structure for Ag-based materials. The coordinates for high-simmetry points for α-Ag_2WO_4 are G (0.0 0.0 0.0), X (0.5 0.0 0.0), Y (0.0 0.5 0.0), Z (0.0 0.0 0.5), U (0.5 0.0 0.5), T (0.0 0.5 0.5), R (0.5 0.5 0.5); for β-Ag_2WO_4 are G (0.0 0.0 0.0), M (0.5 0.0 0.0), A (0.0 0.0 0.5), L (0.5 0.0 0.5); for γ-Ag_2WO_4 are G (0.0 0.0 0.0), DT (0.5 0.0 0.0), SM (0.5 0.5 0.0); for α-$AgVO_3$ are G (0.0 0.0 0.0), B (0.5 0.0 0.0), V (0.5 0.5 0.0), A (0.0 0.0 0.5), B (0.5 0.0 0.5), L (0.5 0.5 0.5); for β-$AgVO_3$ are G (0.0 0.0 0.0), B (0.5 0.0 0.0), GP (0.5 0.5 0.0), A (0.0 0.0 0.5), B (0.5 0.0 0.5), GP (0.5 0.5 0.5); for Ag_3PO_4 are G (0.0 0.0 0.0), X (0.5 0.0 0.0), M (0.5 0.5 0.0), R (0.5 0.5 0.5); for α-Ag_2MoO_4 are G (0.0 0.0 0.0), X (0.5 0.0 0.0), M (0.5 0.5 0.0), Z (0.0 0.0 0.5), R (0.5 0.0 0.5), A (0.5 0.5 0.5); for β-Ag_2MoO_4 are G (0.0 0.0 0.0), DT (0.5 0.0 0.0), ST (0.5 0.5 0.0); for Ag_2CrO_4 G (0.0 0.0 0.0), X (0.5 0.0 0.0), Y (0.0 0.5 0.0), S (0.5 0.5 0.0), Z (0.0 0.0 0.5), U (0.5 0.0 0.5), T (0.0 0.5 0.5), R (0.5 0.5 0.5).

which enables verifying whether an inorganic semiconductor can split H_2O molecules generating the hydroxyl radicals (•OH) and/or reduce the O_2 to superoxide radical ($\bullet O_2^-$). Similarly, the comparison with the potential of forming hydroxyl radicals from OH^- ions ($OH^-/\bullet OH$) indicates the possibility of generating this ROS. The CB and VB edges can be calculated from a well-known set of equations (Equations (4) and (5)) which relates the Mulliken electronegativity (χ) of the semiconductor, the normal hydrogen electrode potential (E_e, NHE = 4.5 eV), and the band gap value (E_{gap}) [100,101].

$$E_{CB} = \chi - E_e - 0.5E_{gap} \quad (4)$$

$$E_{VB} = E_{CB} + E_{gap} \quad (5)$$

The comparison of VB and CB edge potentials with the corresponding potentials of $H_2O/^{\bullet}OH$ (2.72 V at pH = 7, and 1.23 V at pH = 0), $OH^-/\bullet OH$ (2.40 V), and $O_2/\bullet O_2^-$ (−0.33 V) composes Fig. 4. The results for VB edge potentials indicate that the Ag_2WO_4, α-$AgVO_3$, β-Ag_2MoO_4, and Ag_3PO_4 can produce hydroxyl radicals from water molecule splitting at pH = 7. On the other hand, all investigated materials can generate the same radical under pH = 0. Similarly, all simulated materials can oxidize OH^- ions to •OH. The evaluation of CB edge values indicates that the photogenerated charge carriers in α-Ag_2WO_4, α-$AgVO_3$, and β-Ag_2MoO_4 materials reduce O_2 molecules to $\bullet O_2^-$. Such theoretical results are in agreement with the photocatalytic potential reported for Ag_2CrO_4 [49], Ag_2WO_4 [11,23,26], β-Ag_2MoO_4 [46], and Ag_3PO_4 [34,60,87]. In particular, the efficiency of Ag_2CrO_4 as photocatalyst for Rhodamine B degradation under visible radiation was proven by Assis et al. reporting the relation between high photocatalytic activity and morphological properties for such material [113]. Meanwhile, the photocatalytic potential of the other investigated Ag-based semiconductors represents a novel contribution to the literature and potential alternatives to photocatalytic-based goals.

Besides photocatalytic activity, the ability of semiconductor materials to generate ROS is strongly connected to antiviral and antibacterial behavior [114,115]. It comes from the biocide mechanism observed in semiconductors surfaces where the photogenerated ROS are responsible for killing pathogens through oxidative damage to biological compounds or non-oxidative ways, such as autophagy or T-lymphocyte responses [116–123]. Thus, a high concentration of ROS, resulting from the ability of semiconductors to produce such species from reaction with H_2O and O_2 molecules, guarantees a significant antiviral feature as well as a long-time antibacterial activity [96,124,125]. In this work, the biocide activity was accessed from comparing the valence and conduction band edge potentials (Fig. 4) and the potentials to ROS formation; this approach have successfully predicted the biocide properties of $MnMoO_4$ [98]. The results indicate that a good biocide activity is expected for the evaluated Ag-based materials. The biocide activity of some silver semiconductors has previously been evidenced by our group, as observed for α-Ag_2WO_4 [14,23], α-$AgVO_3$ [37,39,41], β-Ag_2MoO_4 [45,46], and Ag_3PO_4 [41] materials. In front of this scenario, the present manuscript represents the first theoretical investigation demonstrating, from ab initio calculations, the ability of these systems to produce ROS and, consequently, to exhibit antiviral and bacterial features found experimentally.

4. Conclusions

This manuscript presents a careful DFT/B3LYP investigation of α-Ag_2WO_4, β-Ag_2WO_4, γ-Ag_2WO_4, α-$AgVO_3$, β-$AgVO_3$, α-Ag_2MoO_4, β-Ag_2MoO_4, Ag_2CrO_4 and Ag_3PO_4 materials. The structural and electronic features of these semiconductors were extensively depicted, and potential antiviral and antibacterial properties were found for materials bulk. The main conclusions can be summarized as follows:

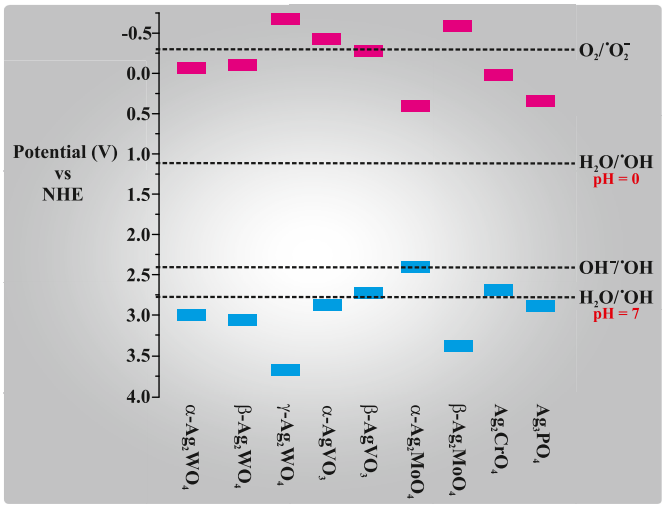

Fig. 4. Calculated valence (blue) and conduction (purple) band edge potentials for α-Ag_2WO_4, β-Ag_2WO_4, γ-Ag_2WO_4, α-$AgVO_3$, β-$AgVO_3$, α-Ag_2MoO_4, β-Ag_2MoO_4, Ag_2CrO_4, and Ag_3PO_4 materials. (For interpretation of the references to colour in this figure legend, the reader is referred to the Web version of this article.)

i) The structural evaluation indicates that the [AgO_x] clusters are structure modifiers in the investigated Ag-based materials, while the [BO_x] clusters behave as structure formers.
ii) DOS and band structure analysis point out all materials as visible-range semiconductors, but β-Ag_2MoO_4, which has a band gap in the ultraviolet region.
iii) The charge carrier features were calculated. The density of holes and electrons suggests that the α-Ag_2MoO_4 is an n-type semiconductor, while the other investigated materials exhibit a p-type semiconductor behavior.
iv) The effective masses evaluation for investigated materials indicates good stability of electron and hole charge carriers for α-Ag_2WO_4, β-Ag_2WO_4, α-$AgVO_3$, β-$AgVO_3$, β-Ag_2MoO_4, Ag_2CrO_4, and Ag_3PO_4 materials
v) The conduction band and valence band edge potentials indicate exciting photocatalytic, antiviral, and antibacterial properties for Ag-based semiconductors in the bulk phase. Thus, additional surface calculations are required to prove the existence of such features.

Finally, the theoretical results for Ag-based semiconductors depicted in this work represent a relevant contribution to the knowledge of the structural and electronic features of these semiconductors and can also help materials science researchers to choose potential candidates for novel devices and technologies.

CRediT authorship contribution statement

Luis Henrique da Silveira Lacerda: Conceptualization, Data curation, Formal analysis, Investigation, Methodology, Software, Visualization, Writing – original draft, Writing – review & editing, Funding acquisition. **Elson Longo:** Funding acquisition, Project administration, Resources, Writing – review & editing. **Juan Andrés:** Funding acquisition, Project administration, Resources, Writing – review & editing. **Miguel Angel San-Miguel:** Funding acquisition, Project administration, Supervision, Resources, Writing – review & editing.

Declaration of competing interest

The authors declare that they have no known competing financial interests or personal relationships that could have appeared to influence

the work reported in this paper.

Acknowledgments

The authors acknowledge support from São Paulo Research Foundation (FAPESP) for grants 2013/07296-2, 2016/23891-6, 2017/26105-4, and 2020/03780-0; from the Coordenação de Aperfeiçoamento de Pessoal de Nível Superior (CAPES); from National Council for Scientific and Technological Development (CNPq) for grant 305792/2020-2.

This work used computational resources of the "Centro Nacional de Processamento de Alto Desempenho em São Paulo" (CENAPAD-SP) and "Centro de Computação John David Rogers" (CCJDR-UNICAMP). The authors acknowledge the National Laboratory for Scientific Computing (LNCC/MCTI, Brazil) for providing HPC resources of the SDumont supercomputer, which have contributed to the research results reported within this work (URL: http://sdumont.lncc.br). The authors also acknowledge Professor. Dr. Sergio Ricardo de Lazaro (UEPG) for the computational facilities of Grupo de Simulação Química (GSQ). Juan Andres acknowledges Universitat Jaume I for project UJI-B2019-30, Generalitat Valenciana for project AICO2020, and Ministerio de Ciencia, Innovación y Universidades (Spain) project PGC2018- 094417-B-I00 for supporting this research financially.

Appendix A. Supplementary data

Additional information of the relative errors observed on the determination of the structural parameters of Ag-based semiconductors can be found in Electronic Supplementary Material.

Supplementary data to this article can be found online at https://doi.org/10.1016/j.jssc.2021.122670.

References

[1] A.F. Gouveia, L. Gracia, E. Longo, M.A. San-Miguel, J. Andrés, Modulating the properties of multifunctional semiconductors by means of morphology: theory meets experiments, Comput. Mater. Sci. 188 (2021) 110217.
[2] L.H.d.S. Lacerda, S.R. de Lazaro, Surface and morphology investigation of FeCrO3 material in ilmenite-, corundum- and lithium niobate- polymorphs, Surf. Interfac. (2020) 100837.
[3] C. Zhaoqiang, P. MohammadJavad, D. Shuxiang, Review of multi-layered magnetoelectric composite materials and devices applications, J. Phys. Appl. Phys. 51 (24) (2018) 243001–243021.
[4] N. Ortega, K. Ashok, J.F. Scott, S.K. Ram, Multifunctional magnetoelectric materials for device applications, J. Phys. Condens. Matter 27 (50) (2015) 504002–504024.
[5] F. Oba, Y. Kumagai, Design and exploration of semiconductors from first principles: a review of recent advances, APEX 11 (6) (2018), 060101.
[6] K.J. Yu, Z. Yan, M. Han, J.A. Rogers, Inorganic semiconducting materials for flexible and stretchable electronics, NPJ Flex. Electron. 1 (1) (2017) 4.
[7] M. Xie, T. Zhang, A novel efficient visible-light-driven double Z-scheme PANI/Ag3PO4/CNO heterojunction photocatalyst mediated by PANI and in situ grown AgNPs, J. Mater. Sci. 55 (2019) 3974–3990.
[8] W. Lin, S. Zhang, D. Wang, C. Zhang, D. Sun, Ultrasound-assisted synthesis of high-efficiency Ag3PO4/CeO2 heterojunction photocatalyst, Ceram. Int. 41 (7) (2015) 8956–8963.
[9] T. Hisatomi, K. Domen, Reaction systems for solar hydrogen production via water splitting with particulate semiconductor photocatalysts, Nat. Catal. 2 (5) (2019) 387–399.
[10] G.G.d. Toledo, V.H. Toledo, A.J.C. Lanfredi, M. Escote, A. Champi, M.C.C.d. Silva, I.L. Nantes-Cardoso, Promising nanostructured materials against enveloped virus, An Acad. Bras Ciências 92 (4) (2020).
[11] R. Alvarez-Roca, A.F. Gouveia, C.C. de Foggi, P.S. Lemos, L. Gracia, L.F. da Silva, C.E. Vergani, M. San-Miguel, E. Longo, J. Andrés, Selective synthesis of α-, β-, and γ-Ag2WO4 polymorphs: promising platforms for photocatalytic and antibacterial materials, Inorg. Chem. 60 (2) (2021) 1062–1079.
[12] L.F. da Silva, A.C. Catto, W. Avansi, L.S. Cavalcante, J. Andrés, K. Aguir, V.R. Mastelaro, E. Longo, A novel ozone gas sensor based on one-dimensional (1D) α-Ag2WO4 nanostructures, Nanoscale 6 (8) (2014) 4058–4062.
[13] L.O. Laier, M. Assis, C.C. Foggi, A.F. Gouveia, C.E. Vergani, L.C.L. Santana, L.S. Cavalcante, J. Andrés, E. Longo, Surface-dependent properties of α-Ag2WO4: a joint experimental and theoretical investigation, Theor. Chem. Accounts 139 (7) (2020) 108.
[14] M. Assis, T. Robeldo, C.C. Foggi, A.M. Kubo, G. Mínguez-Vega, E. Condoncillo, H. Beltran-Mir, R. Torres-Mendieta, J. Andrés, M. Oliva, C.E. Vergani, P.A. Barbugli, E.R. Camargo, R.C. Borra, E. Longo, Ag nanoparticles/α-Ag2WO4 composite formed by electron beam and femtosecond irradiation as potent antifungal and antitumor agents, Sci. Rep. 9 (1) (2019) 9927.
[15] C.C. Foggi, M.T. Fabbro, L.P.S. Santos, Y.V.B. de Santana, C.E. Vergani, A.L. Machado, E. Cordoncillo, J. Andrés, E. Longo, Synthesis and evaluation of α-Ag2WO4 as novel antifungal agent, Chem. Phys. Lett. 674 (2017) 125–129.
[16] M. Mondego, R.C. de Oliveira, M. Penha, M.S. Li, E. Longo, Blue and red light photoluminescence emission at room temperature from CaTiO3 decorated with α-Ag2WO4, Ceram. Int. 43 (7) (2017) 5759–5766.
[17] E. Longo, D.P. Volanti, V.M. Longo, L. Gracia, I.C. Nogueira, M.A.P. Almeida, A.N. Pinheiro, M.M. Ferrer, L.S. Cavalcante, J. Andrés, Toward an understanding of the growth of Ag filaments on α-Ag2WO4 and their photoluminescent properties: a combined experimental and theoretical study, J. Phys. Chem. C 118 (2) (2014) 1229–1239.
[18] I.M. Pinatti, G.R. Fern, E. Longo, T.G. Ireland, P.F.S. Pereira, I.L.V. Rosa, J. Silver, Luminescence properties of α-Ag2WO4 nanorods co-doped with Li+ and Eu3+ cations and their effects on its structure, J. Lumin. 206 (2019) 442–454.
[19] I.M. Pinatti, I.C. Nogueira, W.S. Pereira, P.F.S. Pereira, R.F. Gonçalves, J.A. Varela, E. Longo, I.L.V. Rosa, Structural and photoluminescence properties of Eu3+ doped α-Ag2WO4 synthesized by the green coprecipitation methodology, Dalton Trans. 44 (40) (2015) 17673–17685.
[20] L.S. Cavalcante, M.A.P. Almeida, W. Avansi, R.L. Tranquilin, E. Longo, N.C. Batista, V.R. Mastelaro, M.S. Li, Cluster coordination and photoluminescence properties of α-Ag2WO4 microcrystals, Inorg. Chem. 51 (20) (2012) 10675–10687.
[21] E. Longo, L.S. Cavalcante, D.P. Volanti, A.F. Gouveia, V.M. Longo, J.A. Varela, M.O. Orlandi, J. Andrés, Direct in Situ Observation of the Electron-driven Synthesis of Ag Filaments on α-Ag2WO4 Crystals, vol. 3, 2013, p. 1676.
[22] P.S. Lemos, A. Altomare, A.F. Gouveia, I.C. Nogueira, L. Gracia, R. Llusar, J. Andrés, E. Longo, L.S. Cavalcante, Synthesis and characterization of metastable β-Ag2WO4: an experimental and theoretical approach, Dalton Trans. 45 (3) (2016) 1185–1191.
[23] R.A. Roca, J.C. Sczancoski, I.C. Nogueira, M.T. Fabbro, H.C. Alves, L. Gracia, L.P.S. Santos, C.P. de Sousa, J. Andrés, G.E. Luz, E. Longo, L.S. Cavalcante, Facet-dependent photocatalytic and antibacterial properties of α-Ag2WO4 crystals: combining experimental data and theoretical insights, Catal. Sci. Technol. 5 (8) (2015) 4091–4107.
[24] V.M. Longo, C.C. De Foggi, M.M. Ferrer, A.F. Gouveia, R.S. André, W. Avansi, C.E. Vergani, A.L. Machado, J. Andrés, L.S. Cavalcante, A.C. Hernandes, E. Longo, Potentiated electron transference in α-Ag2WO4 microcrystals with Ag nanofilaments as microbial agent, J. Phys. Chem. 118 (31) (2014) 5769–5778.
[25] N.G. Macedo, T.R. Machado, R.A. Roca, M. Assis, C.C. Foggi, V. Puerto-Belda, G. Mínguez-Vega, A. Rodrigues, M.A. San-Miguel, E. Cordoncillo, H. Beltrán-Mir, J. Andrés, E. Longo, Tailoring the bactericidal activity of Ag nanoparticles/α-Ag2WO4 composite induced by electron beam and femtosecond laser irradiation: integration of experiment and computational modeling, ACS Appl. Bio Mater. 2 (2) (2019) 824–837.
[26] N.G. Macedo, A.F. Gouveia, R.A. Roca, M. Assis, L. Gracia, J. Andrés, E.R. Leite, E. Longo, Surfactant-Mediated morphology and photocatalytic activity of α-Ag2WO4 material, J. Phys. Chem. C 122 (15) (2018) 8667–8679.
[27] Z. Yi, J. Ye, N. Kikugawa, T. Kako, S. Ouyang, H. Stuart-Williams, H. Yang, J. Cao, W. Luo, Z. Li, Y. Liu, R.L. Withers, An orthophosphate semiconductor with photooxidation properties under visible-light irradiation, Nat. Mater. 9 (7) (2010) 559–564.
[28] T. Yan, W. Guan, Y. Xiao, J. Tian, Z. Qiao, H. Zhai, W. Li, J. You, Effect of thermal annealing on the microstructures and photocatalytic performance of silver orthophosphate: the synergistic mechanism of Ag vacancies and metallic Ag, Appl. Surf. Sci. 391 (2017) 592–600.
[29] D.J. Martin, G. Liu, S.J.A. Moniz, Y. Bi, A.M. Beale, J. Ye, J. Tang, Efficient visible driven photocatalyst, silver phosphate: performance, understanding and perspective, Chem. Soc. Rev. 44 (21) (2015) 7808–7828.
[30] B. Liu, Y. Fang, Z. Li, S. Xu, Visible-Light nanostructured photocatalysts–A review, J. Nanosci. Nanotechnol. 15 (2) (2015) 889–920.
[31] X. Ma, J. Yan, N. Liu, L. Zhu, B. Wang, C. Huang, H. Lü, Effect of relaxation on the energetics and electronic structure of clean Ag_3PO_4(111) surface, J. Semiconduct. 37 (3) (2016), 033001.
[32] A.B. Trench, T.R. Machado, A.F. Gouveia, M. Assis, L.G. da Trindade, C. Santos, A. Perrin, C. Perrin, M. Oliva, J. Andrés, E. Longo, Connecting structural, optical, and electronic properties and photocatalytic activity of Ag3PO4:Mo complemented by DFT calculations, Appl. Catal. B Environ. 238 (2018) 198–211.
[33] C.-N. He, W.-Q. Huang, L. Xu, Y.-C. Yang, B.-X. Zhou, G.-F. Huang, P. Peng, W.-M. Liu, Tuning near-gap electronic structure, interface charge transfer and visible light response of hybrid doped graphene and Ag3PO4 composite: dopant effects, Sci. Rep. 6 (1) (2016) 22267.
[34] J.F. Cruz-Filho, T.M.S. Costa, M.S. Lima, L.J. Silva, R.S. Santos, L.S. Cavalcante, E. Longo, G.E. Luz, Effect of different synthesis methods on the morphology, optical behavior, and superior photocatalytic performances of Ag3PO4 sub-microcrystals using white-light-emitting diodes, J. Photochem. Photobiol. Chem. 377 (2019) 14–25.
[35] Q. Liu, N. Li, Z. Qiao, W. Li, L. Wang, S. Zhu, Z. Jing, T. Yan, The multiple promotion effects of ammonium phosphate-modified Ag(3)PO(4) on photocatalytic performance, Front. Chem. 7 (2019) 866.
[36] Y. Seo, K. Park, Y. Hong, E.S. Lee, S.-S. Kim, Y.-T. Jung, H. Park, C. Kwon, Y.-S. Cho, Y.-D. Huh, Reactive-oxygen-species-mediated mechanism for photoinduced antibacterial and antiviral activities of Ag3PO4, J. Anal. Sci. Technol. 11 (1) (2020) 21.

[37] B.N.A.d.S. Pimentel, C.C. de Foggi, P.A. Barbugli, R.C. de Oliveira, E.D. de Avila, E. Longo, C.E. Vergani, Antifungal activity and biocompatibility of α-AgVO3 microcrystals: a promising material against oral Candida disease, Mater. Sci. Eng. C 108 (2020) 110405.

[38] A. Beltrán, L. Gracia, J. Andrés, E. Longo, First-principles study on polymorphs of AgVO3: assessing to structural stabilities and pressure-induced transitions, J. Phys. Chem. C 121 (49) (2017) 27624–27642.

[39] R.C. Oliveira, M.M. Teixeira, J.P.C. Costa, M. Penha, E.M. Francisco, J.S. da Silva, M.S. Li, E. Longo, L. Gracia, J. Andrés, α- and β-AgVO3 polymorphs as photoluminescent materials: an example of temperature-driven synthesis, Ceram. Int. 44 (6) (2018) 5939–5944.

[40] J. Soares da Silva, T.R. Machado, T.A. Martins, M. Assis, C.C. Foggi, N.G. Macedo, H. Beltrán-Mir, E. Cordoncillo, J. Andrés, E. Longo, α-AgVO3 decorated by hydroxyapatite (Ca10(PO4)6(OH)2): tuning its photoluminescence emissions and bactericidal activity, Inorg. Chem. 58 (9) (2019) 5900–5913.

[41] R.C. de Oliveira, C.C. de Foggi, M.M. Teixeira, M.D.P. da Silva, M. Assis, E.M. Francisco, B.N.A.d.S. Pimentel, P.F.d.S. Pereira, C.E. Vergani, A.L. Machado, J. Andres, L. Gracia, E. Longo, Mechanism of antibacterial activity via morphology change of α-AgVO3: theoretical and experimental insights, ACS Appl. Mater. Interfaces 9 (13) (2017) 11472–11481.

[42] A. Beltrán, L. Gracia, E. Longo, J. Andrés, First-principles study of pressure-induced phase transitions and electronic properties of Ag2MoO4, J. Phys. Chem. C 118 (7) (2014) 3724–3732.

[43] A.F. Gouveia, J.C. Sczancoski, M.M. Ferrer, A.S. Lima, M.R.M.C. Santos, M.S. Li, R.S. Santos, E. Longo, L.S. Cavalcante, Experimental and theoretical investigations of electronic structure and photoluminescence properties of β-Ag2MoO4 microcrystals, Inorg. Chem. 53 (11) (2014) 5589–5599.

[44] F.S. Cunha, J.C. Sczancoski, I.C. Nogueira, V.G. de Oliveira, S.M.C. Lustosa, E. Longo, L.S. Cavalcante, Structural, morphological and optical investigation of β-Ag2MoO4 microcrystals obtained with different polar solvents, CrystEngCommCrystEngComm 17 (43) (2015) 8207–8211.

[45] C.C. De Foggi, R.C. De Oliveira, M. Assis, M.T. Fabbro, V.R. Mastelaro, C.E. Vergani, L. Gracia, J. Andrés, E. Longo, A.L. Machado, Unvealing the role of β-Ag2MoO4 microcrystals to the improvement of antibacterial activity, Mater. Sci. Eng. C 111 (2020) 110765.

[46] C.A. Oliveira, D.P. Volanti, A.E. Nogueira, C.A. Zamperini, C.E. Vergani, E. Longo, Well-designed β-Ag2MoO4 crystals with photocatalytic and antibacterial activity, Mater. Des. 115 (2017) 73–81.

[47] G.S. Silva, L. Gracia, M.T. Fabbro, L.P. Serejo dos Santos, H. Beltrán-Mir, E. Cordoncillo, E. Longo, J. Andrés, Theoretical and experimental insight on Ag2CrO4 microcrystals: synthesis, characterization, and photoluminescence properties, Inorg. Chem. 55 (17) (2016) 8961–8970.

[48] F. Yu, D. Nan, B. Wang, Z. Liu, Y. Li, L. He, X. Tang, J. Zhang, Catalytic properties of the composite of La-doped ZnO nanorods and Ag2CrO4 nanoparticles, Appl. Phys. A 126 (7) (2020) 482.

[49] M. Miclau, S. Kumar, D. Ursu, C. Orha, N. Miclau, J.-M. Rueff, S. Malo, C. Martin, Ag2CrO4 for photocatalytic applications: high performance of crystals designed by autogenous pressure, Mater. Char. 158 (2019) 109970.

[50] I.M. Pinatti, A.C.M. Tello, A.B. Trench, C.C. de Foggi, P.F.S. Pereira, M.M. Teixeira, N. Jacomaci, J. Andrés, E. Longo, Zinc-substituted Ag2CrO4: a material with enhanced photocatalytic and biological activity, J. Alloys Compd. 835 (2020) 155315.

[51] K. Burke, Perspective on density functional theory, J. Chem. Phys. 136 (15) (2012) 150901–150909.

[52] A.D. Becke, Perspective: fifty years of density-functional theory in chemical physics, J. Chem. Phys. 140 (18) (2014) 18A301–18A320.

[53] M. Batvandi, A. Haghighatzadeh, B. Mazinani, Synthesis of Ag3PO4 microstructures with morphology-dependent optical and photocatalytic behaviors, Appl. Phys. A 126 (7) (2020) 571.

[54] R. Dovesi, A. Erba, R. Orlando, C.M. Zicovich-Wilson, B. Civalleri, L. Maschio, M. Rérat, S. Casassa, J. Baima, S. Salustro, B. Kirtman, Quantum-mechanical condensed matter simulations with CRYSTAL, Wiley Interdiscipl. Rev.: Comput. Mol. Sci. 8 (4) (2018) e1360-36.

[55] T.M. Duarte, P.G.C. Buzolin, I.M.G. Santos, E. Longo, J.R. Sambrano, Choice of hybrid functional and basis set optimization to calculate the structural, electronic, mechanical, and vibrational properties of BaSnO3, Theor. Chem. Accounts 135 (6) (2016) 151.

[56] E.O. Gomes, G.S.L. Fabris, M.M. Ferrer, F.V. Motta, M.R.D. Bomio, J. Andres, E. Longo, J.R. Sambrano, Computational procedure to an accurate DFT simulation to solid state systems, Comput. Mater. Sci. 170 (2019) 109176.

[57] L. Brugnoli, A.M. Ferrari, B. Civalleri, A. Pedone, M.C. Menziani, Assessment of density functional approximations for highly correlated oxides: the case of CeO2 and Ce2O3, J. Chem. Theor. Comput. 14 (9) (2018) 4914–4927.

[58] S. Grimme, J. Antony, S. Ehrlich, H. Krieg, A consistent and accurate ab initio parametrization of density functional dispersion correction (DFT-D) for the 94 elements H-Pu, J. Chem. Phys. 132 (15) (2010) 154104.

[59] S. Grimme, Semiempirical GGA-type density functional constructed with a long-range dispersion correction, J. Comput. Chem. 27 (15) (2006) 1787–1799.

[60] F. Lipsky, L.H.d.S. Lacerda, S.R. de Lazaro, E. Longo, J. Andrés, M.A. San-Miguel, Unraveling the relationship between exposed surfaces and the photocatalytic activity of Ag3PO4: an in-depth theoretical investigation, RSC Adv. 10 (51) (2020) 30640–30649.

[61] H.J. Monkhorst, J.D. Pack, Special points for Brillouin-zone integrations, Phys. Rev. B 13 (12) (1976) 5188–5192.

[62] C. Pisani, R. Dovesi, C. Roetti, Hartree-Fock Ab Initio Treatment of Crystalline Systems, Springer Berlin Heidelberg, 1988.

[63] M.D. Towler, N.L. Allan, N.M. Harrison, V.R. Saunders, W.C. Mackrodt, E. Aprà, Ab initio study of MnO and NiO, Phys. Rev. B 50 (8) (1994) 5041–5054.

[64] A.M. Ferrari, C. Pisani, An ab initio periodic study of NiO supported at the Pd (100) surface. Part 1:The perfect epitaxial monolayer, J. Phys. Chem. B 110 (15) (2006) 7909–7917.

[65] E. Ruiz, M. Llunell, P. Alemany, Calculation of exchange coupling constants in solid state transition metal compounds using localized atomic orbital basis sets, J. Solid State Chem. 176 (2) (2003) 400–411.

[66] E. Aprà, E. Stefanovich, R. Dovesi, C. Roetti, An ab initio Hartree—fock study of silver chloride, Chem. Phys. Lett. 186 (4) (1991) 329–335.

[67] F. Corà, A. Patel, N.M. Harrison, R. Dovesi, C.R.A. Catlow, An ab initio Hartree−Fock study of the cubic and tetragonal phases of bulk tungsten trioxide, J. Am. Chem. Soc. 118 (48) (1996) 12174–12182.

[68] F. Cora, A. Patel, N.M. Harrison, C. Roetti, C. Richard A. Catlow, An ab initio Hartree–Fock study of α-MoO3, J. Mater. Chem. 7 (6) (1997) 959–967.

[69] R.A. Roca, P.S. Lemos, L. Gracia, J. Andrés, E. Longo, Uncovering the metastable γ-Ag2WO4 phase: a joint experimental and theoretical study, RSC Adv. 7 (10) (2017) 5610–5620.

[70] M.T. Galante, P. Sotelo, M.K. Hossain, A. Vali, A. Raamann, C. Longo, R.T. Macaluso, K. Rajeshwar, Silver oxide-based semiconductors for solar fuels production and environmental remediation: a solid-state chemistry approach, ChemElectroChem 6 (1) (2019) 87–96.

[71] R. Guo, G. Han, A. Yan, Y. He, N. Su, X. Liu, T. Yi, Epitaxial growth of metastable phase α-Ag2MoO4 on WO3 surface: visible light-driven photocatalysis, sterilization, and reaction mechanism, J. Alloys Compd. 814 (2020) 152255.

[72] S.d. Lazaro, J. Milanez, A.T.d. Figueiredo, V.M. Longo, V.R. Mastelaro, F.S.D. Vicente, A.C. Hernandes, J.A. Varela, E. Longo, Relation between photoluminescence emission and local order-disorder in the, CaTiO3 lattice modifier 90 (11) (2007) 111904.

[73] P.T. Diallo, K. Jeanlouis, P. Boutinaud, R. Mahiou, J.C. Cousseins, Improvement of the optical performances of Pr3+ in CaTiO3, J. Alloys Compd. 323–324 (2001) 218–222.

[74] P.R.d. Lucena, F.M. Pontes, C.D. Pinheiro, E. Longo, P.S. Pizani, S. Lázaro, A.G. Souza, I.M.G.d. Santos, Photoluminescence in disordered materials, Cerâmica 50 (2004) 138–144.

[75] G. Botelho, J.C. Sczancoski, J. Andres, L. Gracia, E. Longo, Experimental and theoretical study on the structure, optical properties, and growth of metallic silver nanostructures in Ag3PO4, J. Phys. Chem. C 119 (11) (2015) 6293–6306.

[76] S. Mishra, B. Ganguli, Effect of Na substitution on electronic and optical properties of CuInS2 chalcopyrite semiconductor, J. Solid State Chem. 232 (2015) 131–137.

[77] S. Mishra, B. Ganguli, Effects of Structural Distortion on Electronic and Optical Properties of Defect $CdGa_2X_4$ (X = S, Se, Te) Chalcopyrite Semiconductor, 2012.

[78] J.C. Sczancoski, S. Maya-Johson, W. da Silva Pereira, E. Longo, E.R. Leite, Atomic diffusion induced by electron-beam irradiation: an in situ study of Ag structures grown from α-Ag2WO4, Cryst. Growth Des. 19 (1) (2019) 106–115.

[79] J. Andrés, M.M. Ferrer, L. Gracia, A. Beltran, V.M. Longo, G.H. Cruvinel, R.L. Tranquilin, E. Longo, A combined experimental and theoretical study on the formation of Ag filaments on β-Ag2MoO4 induced by electron irradiation, Part. Part. Syst. Char. 32 (6) (2015) 646–651.

[80] J.P.d.C.d. Costa, M. Assis, V. Teodoro, A. Rodrigues, C. Cristina de Foggi, M.A. San-Miguel, J.P. Pereira do Carmo, J. Andrés, E. Longo, Electron beam irradiation for the formation of thick Ag film on Ag3PO4, RSC Adv. 10 (37) (2020) 21745–21753.

[81] W.d.S. Pereira, J. Andrés, L. Gracia, M.A. San-Miguel, E.Z. da Silva, E. Longo, V.M. Longo, Elucidating the real-time Ag nanoparticle growth on α-Ag2WO4 during electron beam irradiation: experimental evidence and theoretical insights, Phys. Chem. Chem. Phys. 17 (7) (2015) 5352–5359.

[82] R.C. de Oliveira, M. Assis, M.M. Teixeira, M.D.P. da Silva, M.S. Li, J. Andres, L. Gracia, E. Longo, An experimental and computational study of β-AgVO3: optical properties and formation of Ag nanoparticles, J. Phys. Chem. C 120 (22) (2016) 12254–12264.

[83] R.A. Roca, A.F. Gouveia, P.S. Lemos, L. Gracia, J. Andrés, E. Longo, formation of Ag nanoparticles on β-Ag2WO4 through electron beam irradiation: a synergetic computational and experimental study, Inorg. Chem. 55 (17) (2016) 8661–8671.

[84] M.T. Fabbro, C. Saliby, L.R. Rios, F.A. La Porta, L. Gracia, M.S. Li, J. Andrés, L.P.S. Santos, E. Longo, Identifying and rationalizing the morphological, structural, and optical properties of β-Ag2MoO4 microcrystals, and the formation process of Ag nanoparticles on their surfaces: combining experimental data and first-principles calculations, Sci. Technol. Adv. Mater. 16 (6) (2015), 065002.

[85] M.A. San-Miguel, E.Z. da Silva, S.M. Zanetti, M. Cilense, M.T. Fabbro, L. Gracia, J. Andrés, E. Longo, In situ growth of Ag nanoparticles onα-Ag2WO4under electron irradiation: probing the physical principles, Nanotechnology 27 (22) (2016) 225703.

[86] L.P. S, S.G. S, R.R. A, A. M, T.-M. R, B.-M. H, M.-V. G, C. E, A. J, L. E, Laser and electron beam-induced formation of Ag/Cr structures on Ag2CrO4, Phys. Chem. Chem. Phys. 21 (11) (2019) 6101–6111.

[87] G. Botelho, J. Andres, L. Gracia, L.S. Matos, E. Longo, Photoluminescence and photocatalytic properties of Ag3PO4 microcrystals: an experimental and theoretical investigation, ChemPlusChem 81 (2) (2016) 202–212.

[88] C.C. dos Santos, M. de Assis, T.R. Machado, P.F. dos Santos Pereira, G. Minguez-Vega, E. Cordoncillo, H. Beltran-Mir, C. Doñate-Buendía, J. Andrés, E. Longo, Proof-of-Concept studies directed toward the formation of metallic Ag nanostructures from Ag3PO4 induced by electron beam and femtosecond laser, Part. Part. Syst. Char. 36 (6) (2019) 1800533.

[89] J. Andrés, L. Gracia, P. Gonzalez-Navarrete, V.M. Longo, W. Avansi Jr., D.P. Volanti, M.M. Ferrer, P.S. Lemos, F.A. La Porta, A.C. Hernandes, E. Longo,

Structural and Electronic Analysis of the Atomic Scale Nucleation of Ag on α-Ag2WO4 Induced by Electron Irradiation, vol. 4, 2014, p. 5391.
[90] C. Freysoldt, B. Grabowski, T. Hickel, J. Neugebauer, G. Kresse, A. Janotti, C.G. Van de Walle, First-principles calculations for point defects in solids, Rev. Mod. Phys. 86 (1) (2014) 253–305.
[91] Y. Kumagai, M. Choi, Y. Nose, F. Oba, First-principles study of point defects in chalcopyrite $SnSnP_2$, Phys. Rev. B 90 (12) (2014) 125202.
[92] C. Persson, Y.-J. Zhao, S. Lany, A. Zunger, n-type doping of $CuInSe_2$ and $CuGaSe_2$, Phys. Rev. B 72 (3) (2005), 035211.
[93] R. Sun, M.K.Y. Chan, S. Kang, G. Ceder, Intrinsic stoichiometry and oxygen-induced p-type conductivity of pyrite FeS_2, Phys. Rev. B 84 (3) (2011), 035212.
[94] L.H.d.S. Lacerda, S.R.R. de Lazaro, M.A. San-Miguel, Surface and morphological study of LiNbO3: p-type semiconductivity on stoichiometric surfaces, New J. Chem. (2021) 16594–16605.
[95] L.H.d.S. Lacerda, M.A. San-Miguel, S.R. de Lazaro, Surface and morphological studies of LiNbO3: p-type semiconductivity on stoichiometric surfaces, New J. Chem. 45 (36) (2021) 16594–16605.
[96] P.D. Rakowska, M. Tiddia, N. Faruqui, C. Bankier, Y. Pei, A.J. Pollard, J. Zhang, I.S. Gilmore, Antiviral surfaces and coatings and their mechanisms of action, Commun. Mater. 2 (1) (2021) 53.
[97] C.-S. Tan, Y.-J. Chen, C.-F. Hsia, M.H. Huang, Facet-Dependent Electrical Conductivity Properties of Silver Oxide Crystals 12 (3) (2017) 293–297.
[98] L.H.d.S. Lacerda, M.A. San-Miguel, DFT approaches unraveling the surface and morphological properties of MnMoO4, Appl. Surf. Sci. (2021) 150882.
[99] L.H.S. Lacerda, S.R. de Lazaro, Density Functional Theory investigation of rhombohedral multiferroic oxides for photocatalytic water splitting and organic photodegradation, J. Photochem. Photobiol. Chem. 400 (2020).
[100] J.J. Liu, X.L. Fu, S.F. Chen, Y.F. Zhu, Electronic structure and optical properties of Ag3PO4 photocatalyst calculated by hybrid density functional method, Appl. Phys. Lett. 99 (19) (2011) 191903.
[101] M. Mousavi, A. Habibi-Yangjeh, M. Abitorabi, Fabrication of novel magnetically separable nanocomposites using graphitic carbon nitride, silver phosphate and silver chloride and their applications in photocatalytic removal of different pollutants using visible-light irradiation, J. Colloid Interface Sci. 480 (2016) 218–231.
[102] J. Yu, P. Zhou, Q. Li, New insight into the enhanced visible-light photocatalytic activities of B-, C- and B/C-doped anatase TiO_2 by first-principles, Phys. Chem. Chem. Phys. 15 (29) (2013) 12040–12047.
[103] P. Zhou, J. Yu, Y. Wang, The new understanding on photocatalytic mechanism of visible-light response NS codoped anatase TiO_2 by first-principles, Appl. Catal. B Environ. 142–143 (2013) 45–53.
[104] X. Ma, Y. Dai, M. Guo, B. Huang, The role of effective mass of carrier in the photocatalytic behavior of silver halide-based Ag@AgX (X = Cl, Br, I): a theoretical study, ChemPhysChem 13 (9) (2012) 2304–2309.
[105] G.B. Soares, R.A.P. Ribeiro, S.R. de Lazaro, C. Ribeiro, Photoelectrochemical and theoretical investigation of the photocatalytic activity of TiO_2:N, RSC Adv. 6 (92) (2016) 89687–89698.
[106] N. Gao, C. Quan, Y. Ma, Y. Han, Z. Wu, W. Mao, J. Zhang, J. Yang, X.a. Li, W. Huang, Experimental and first principles investigation of the multiferroics $BiFeO_3$ and $Bi_{0.9}Ca_{0.1}FeO_3$: structure, electronic, optical and magnetic properties, Phys. B Condens. Matter 481 (2016) 45–52.
[107] Y. Gu, J. Zhao, W. Zhang, H. Zheng, L. Liu, W. Chen, Structural transformation and multiferroic properties of Sm and Ti co-doped $BiFeO_3$ ceramics with Fe vacancies, Ceram. Int. 43 (17) (2017) 14666–14671.
[108] A. Das, S. De, S. Bandyopadhyay, S. Chatterjee, D. Das, Magnetic, dielectric and magnetoelectric properties of $BiFeO_3$-$CoFe_2O_4$ nanocomposites, J. Alloys Compd. 697 (2017) 353–360.
[109] T. Murtaza, J. Ali, M.S. Khan, K. Asokan, Structural, electrical and magnetic properties of multiferroic $BiFeO_3$–$SrTiO_3$ composites, J. Mater. Sci. Mater. Electron. 29 (3) (2018) 2110–2119.
[110] W. Xue, D. Huang, X. Wen, S. Chen, M. Cheng, R. Deng, B. Li, Y. Yang, X. Liu, Silver-based semiconductor Z-scheme photocatalytic systems for environmental purification, J. Hazard Mater. 390 (2020) 122128.
[111] S.J.A. Moniz, S.A. Shevlin, D.J. Martin, Z.-X. Guo, J. Tang, Visible-light driven heterojunction photocatalysts for water splitting - a critical review, Energy Environ. Sci. 8 (3) (2015) 731–759.
[112] T. Jing, Y. Dai, X. Ma, W. Wei, B. Huang, Electronic structure and photocatalytic water-splitting properties of $Ag_2ZnSn(S_{1-x}Se_x)_4$, J. Phys. Chem. C 119 (2015) 27900–27908.
[113] M. Assis, C.C. de Foggi, V. Teodoro, J.P. de Campos da Costa, C.E. Silva, T. Robeldo, P.F. Caperucci, C.E. Vergani, R.C. Borra, I. Sorribes, A.F. Gouveia, M.A. San-Miguel, J. Andrés, E. Longo, Surface-dependent photocatalytic and biological activities of Ag2CrO4: integration of experiment and simulation, Appl. Surf. Sci. 545 (2021) 148964.
[114] Y. Li, W. Zhang, J. Niu, Y. Chen, Mechanism of photogenerated reactive oxygen species and correlation with the antibacterial properties of engineered metal-oxide nanoparticles, ACS Nano 6 (6) (2012) 5164–5173.
[115] W. He, J. Cai, X. Jiang, J.-J. Yin, Q. Meng, Generation of reactive oxygen species and charge carriers in plasmonic photocatalytic Au@TiO2 nanostructures with enhanced activity, Phys. Chem. Chem. Phys. 20 (23) (2018) 16117–16125.
[116] M. Miyauchi, K. Sunada, K. Hashimoto, Antiviral effect of visible light-sensitive, CuxO/TiO2 Photocatalyst 10 (9) (2020) 1093.
[117] C.N. Paiva, M.T. Bozza, Are reactive oxygen species always detrimental to pathogens? Antioxidants Redox Signal. 20 (6) (2013) 1000–1037.
[118] X. Dong, W. Liang, M.J. Meziani, Y.-P. Sun, L. Yang, Carbon dots as potent antimicrobial agents, Theranostics 10 (2) (2020) 671–686.
[119] D. Olagnier, S. Peri, C. Steel, N. van Montfoort, C. Chiang, V. Beljanski, M. Slifker, Z. He, C.N. Nichols, R. Lin, S. Balachandran, J. Hiscott, Cellular oxidative stress response controls the antiviral and apoptotic programs in Dengue virus-infected dendritic cells, PLoS Pathog. 10 (12) (2014), e1004566.
[120] D. Wang, Y. Zhu, X. Wan, X. Zhang, J. Zhang, Colloidal semiconductor nanocrystals for biological photodynamic therapy applications: recent progress and perspectives, Prog. Nat. Sci.: Mater. Int. 30 (4) (2020) 443–455.
[121] V.P. Skulachev, Possible role of reactive oxygen species in antiviral defense, Biochemistry (Mosc). 63 (12) (1998) 1438–1440.
[122] D. Wang, L. Zhao, H. Ma, H. Zhang, L.-H. Guo, Quantitative analysis of reactive oxygen species photogenerated on metal oxide nanoparticles and their bacteria toxicity: the role of superoxide radicals, Environ. Sci. Technol. 51 (17) (2017) 10137–10145.
[123] A. Sirelkhatim, S. Mahmud, A. Seeni, N.H.M. Kaus, L.C. Ann, S.K.M. Bakhori, H. Hasan, D. Mohamad, Review on zinc oxide nanoparticles: antibacterial activity and toxicity mechanism, Nano-Micro Lett. 7 (3) (2015) 219–242.
[124] L. Chen, J. Liang, An overview of functional nanoparticles as novel emerging antiviral therapeutic agents, Mater. Sci. Eng. C 112 (2020) 110924.
[125] B. Balasubramaniam, Prateek, S. Ranjan, M. Saraf, P. Kar, S.P. Singh, V.K. Thakur, A. Singh, R.K. Gupta, Antibacterial and antiviral functional materials: chemistry and biological activity toward tackling COVID-19-like pandemics, ACS Pharmacol. Transl. Sci. 4 (1) (2021) 8–54.